Construction of Fe regulated NiMoN nanorods as an efficient electrocatalyst for overall water splitting and urea electrolysis

Longlong Liu[a†], Lanli Chen[c†], Huaming Zhang[a*], Muhammad Humayun[b], Yuxiao Liu[d], Junhong Duan[a], Yanjun Fu[a], Mohamed Bououdina[b], Xinying Xue[e*], Chundong Wang[d,b]

[a] Jiangxi Province Key Laboratory of Optoelectronic Information Science and Technology, Nanchang Hangkong University, Nanchang 330063, Jiangxi, China

[b] Energy, Water, and Environment Lab, College of Sciences and Humanities, Prince Sultan University, Riyadh 11586, Saudi Arabia

[c] School of Mathematics and Physics, Hubei Polytechnic University, Huangshi 435003, PR China

[d] School of Integrated Circuits, State Key Laboratory of New Textile Materials and Advanced Processing, Huazhong University of Science and Technology, Wuhan 430074, P.R. China

[e] *Department of Physics, College of Science, Shihezi University, Xinjiang 832003, P.R. China*

Corresponding authors: Huaming Zhang (70451@nchu.edu.cn); Xinying Xue (yyingxx@163.com)

† These authors contributed equally to this work.

1. Experimental and calculation methods

1.1 Characterization

A variety of analytical methods were employed to characterize the composition and microstructure of the obtained samples. The crystalline phases of the catalysts were characterized using X-ray diffraction (XRD) technology over a range of 10 to 80° with a scanning rate of 10° min^{-1}. Field emission scanning electron microscopy (Zeiss-G-300, FESEM) and transmission electron microscopy (TEM; FEI-Tecnai-TM G2F30) were utilized to examine the micromorphology and microstructure of the samples. High-resolution transmission electron microscopy (HR-TEM) and high-angle annular dark-field scanning transmission electron microscopy (HAADF-STEM) were employed to study the microstructure and morphology of the samples. The chemical composition and state of all electrocatalysts were verified using X-ray photoelectron spectroscopy (XPS) with an Al Kα X-ray source (providing photons of 1486.6 eV). The pore distribution and N_2 adsorption/desorption isotherms were determined using an ASAP2460 adsorption-desorption isotherm. The amounts of Fe, Ni and Mo in catalysts were determined by Inductively Coupled Plasma Optical Emission Spectrometry (ICP-OES, Agilent ICPOES 720ES).

1.2 Electrochemical measurement

CHI-760E electrochemical workstation (Chenhua Instruments, Shanghai, China) was used for electrochemical analysis with a typical three-electrode setup. The working electrode was the prepared catalyst (1 × 1 cm^{-2}), a graphite rod served as the counter

electrode, and Hg/HgO saturated with KOH was used as the reference electrode. After obtaining stable cyclic voltammetry (CV) curves through 30 cycles, the polarization curves of the catalysts were analyzed using linear sweep voltammetry (LSV) at a scan rate of 5 mV s^{-1}. For all polarization curves presented in this work, the values were manually corrected for 95% by the formula:

$$E_{RHE} = E_{\mathrm{Hg/HgO}} + 0.059pH + E_{\mathrm{Hg/HgO}} - iRs$$

where E_{RHE} is 0.098 V vs SHE, and the compensated ohmic value comes from the electrochemical impedance spectroscopy (EIS) attachment. The Tafel equation η= blog j + a, where b is the slope and j is the current density, was used to gain more insight into the reaction mechanism. For EIS studies, the potential scan was stopped at different potentials, and the resulting impedance spectra were recorded over a frequency range from 1 MHz to 0.01 Hz. Additionally, the electrochemical active surface area (ECSA) was predicted using the non-Faradaic potential region double-layer capacitance (Cdl), with the ECSA value given by the equation:

$$ECSA = C_{dl}/C_s$$

where $C_s \approx 0.04$ mF cm^{-2}. Here, C_{dl} can be predicted as half of the slope by plotting the relationship between the capacitive current ($\Delta j = j_{anodic} - j_{cathodic}$) and the corresponding scan rate. The stability of the catalysts was determined using the chronopotentiometry method.

1.3 Theoretical calculations

The Vienna ab-initio Simulation Package (VASP) was used to perform the first-

principles calculations based on the density function theory (DFT) [1]. The generalized gradient approximation (GGA) of the Perdew-Burke-Ernzerhof (PBE) form was employed to describe exchange-related interactions [2].

The cutoff energy for the plane-wave basis was set at 450 eV. The convergence criterion was set to be 10^{-5} eV and 0.01 eV/Å for energy and force, respectively. A 4×4×1 mesh of the k-point integration was used.

As shown in Fig. 1, the (100) surface of $Ni_{0.2}Mo_{0.8}N$ was modeled by a 3×3 periodic slab and a vacuum slab of 15 Å along z direction was used to avoid the effect of periodic image interaction. The bottom three layers were fixed and the other layers were relaxed.

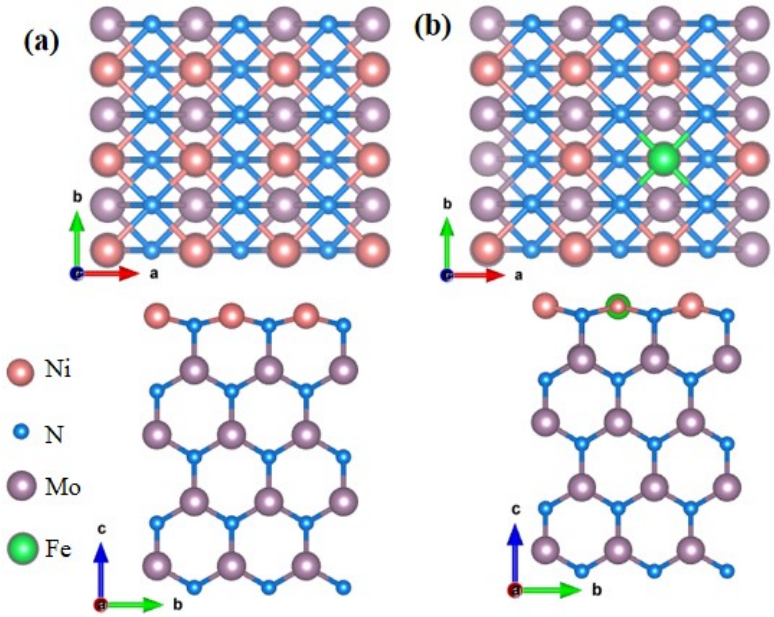

Fig. 1 The top and side views of (a) $Ni_{0.2}Mo_{0.8}N$ and (b) Fe-doped $Ni_{0.2}Mo_{0.8}N$.

Reference

1 G. Kresse, *J. Non-Cryst. Solids*, 1995, **192-193**, 222-229.

2 G. Kresse and J. Furthmüller, *Physical Review B*, 1996, **54**, 11169-11186.

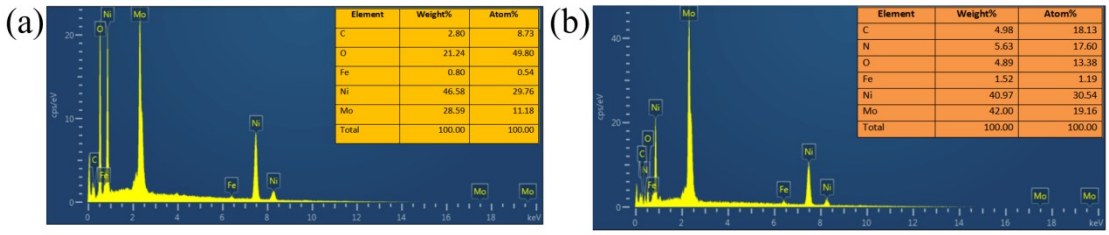

Fig. S1. EDS spectrum of (a)Fe-$NiMoO_4$ and (b)Fe-NiMoN.

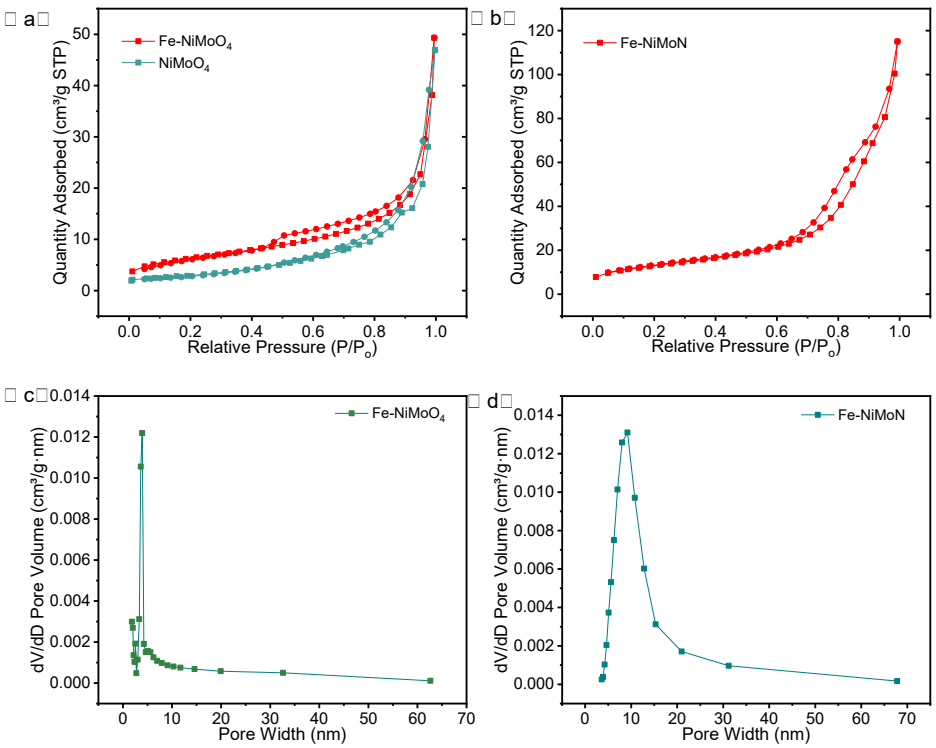

Fig. S2. (a) BET data for $NiMoO_4$ and Fe-$NiMoO_4$. (b) BET data for Fe-NiMoN. Pore width distribution curves for (c) Fe-$NiMoO_4$ and (d) Fe-NiMoN.

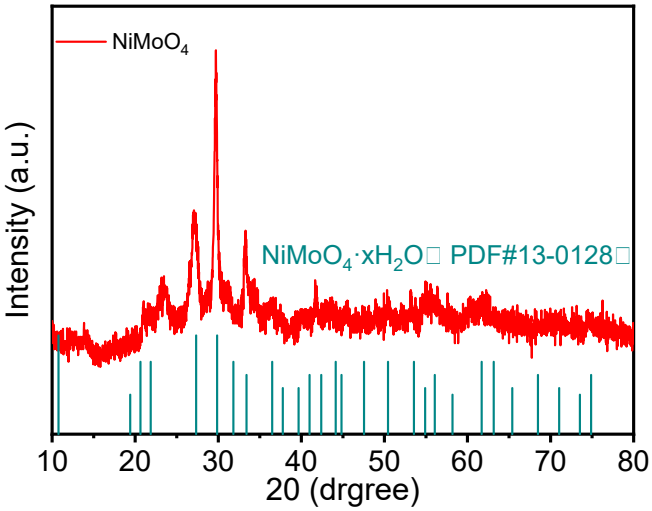

Fig. S3. XRD spectra of $NiMoO_4$.

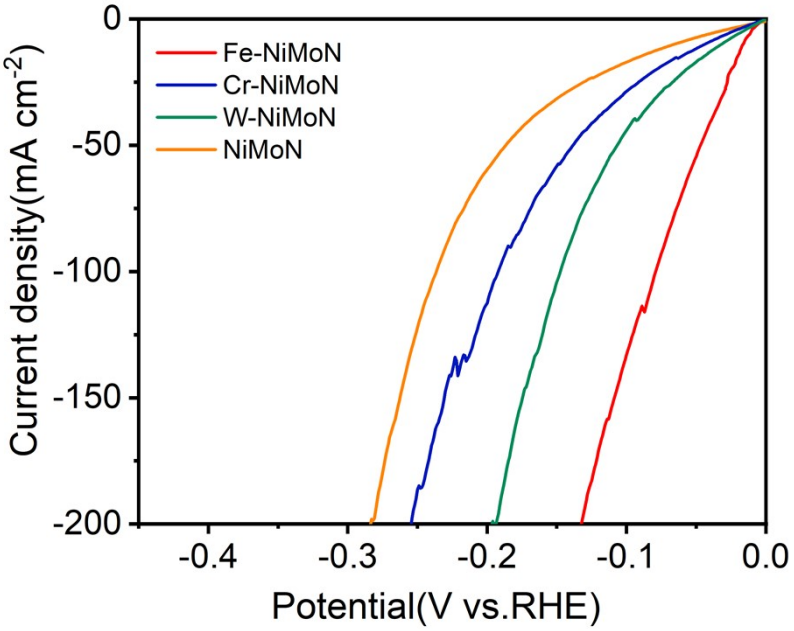

Fig. S4. Polarization HER curves of Fe-NiMoN, Cr-NiMoN, W-NiMoN and NiMoN.

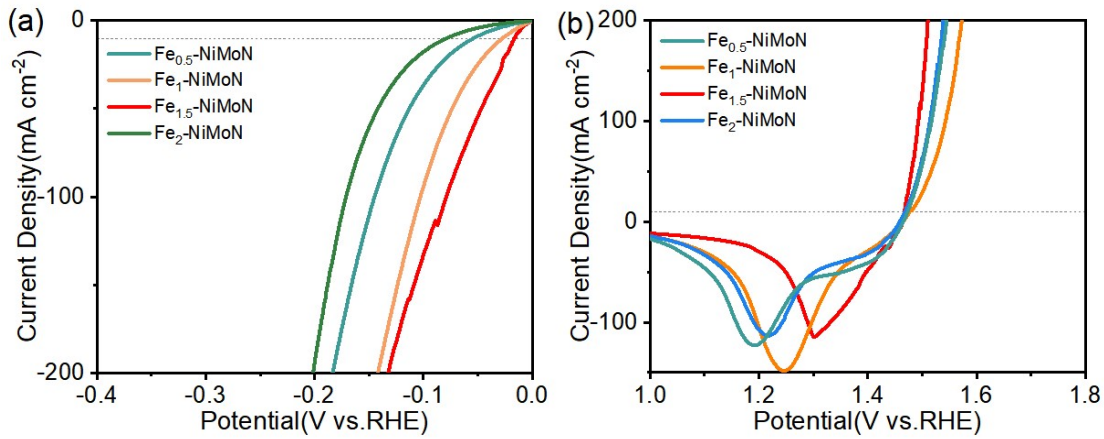

Fig. S5. The HER (a) and OER (b) performance of Fe-NiMoN with different $FeSO_4 \cdot 7H_2O$ contents.

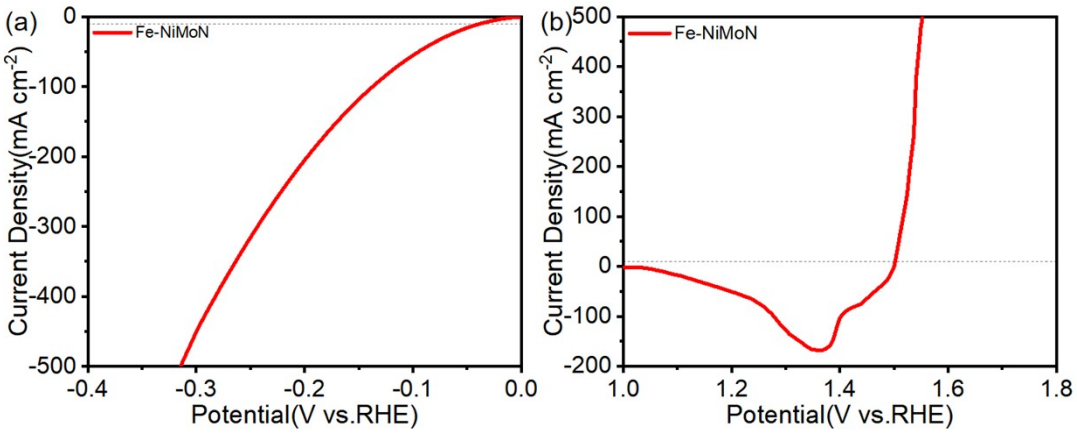

Fig. S6. Polarization LSV curves toward (a) HER and (b) OER.

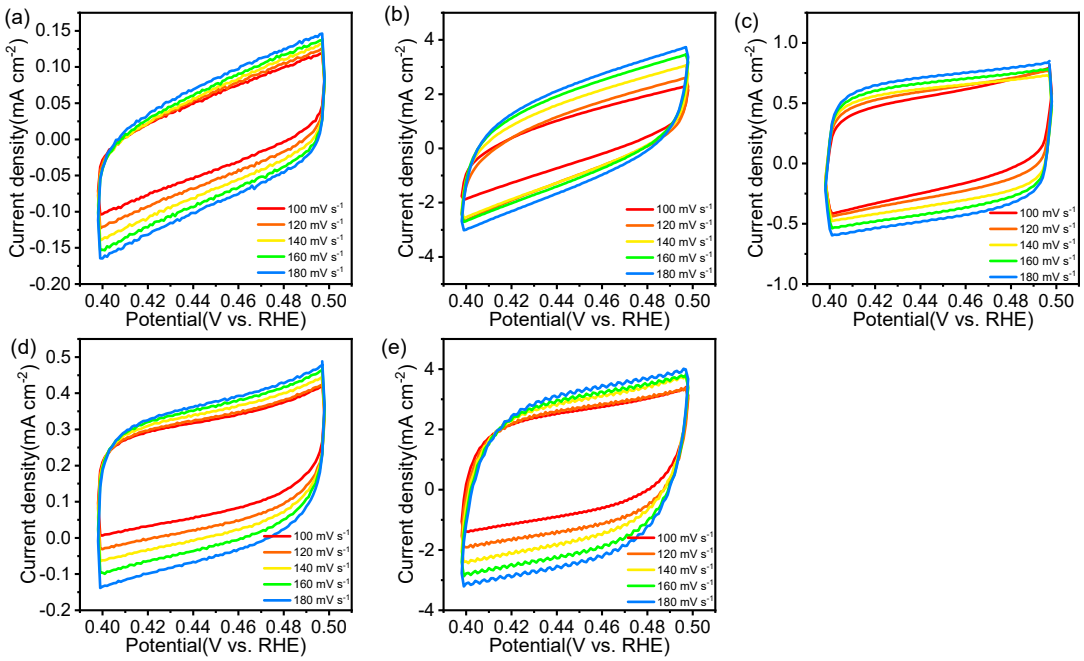

Fig. S7. CV curves of the catalysts recorded in the region of 0.394 ~ 0.494 V vs. RHE at different scan rates. (a) NF, (b) Pt/C, (c)NiMoN , (d) $NiMoO_4$, (e) Fe-NiMoN

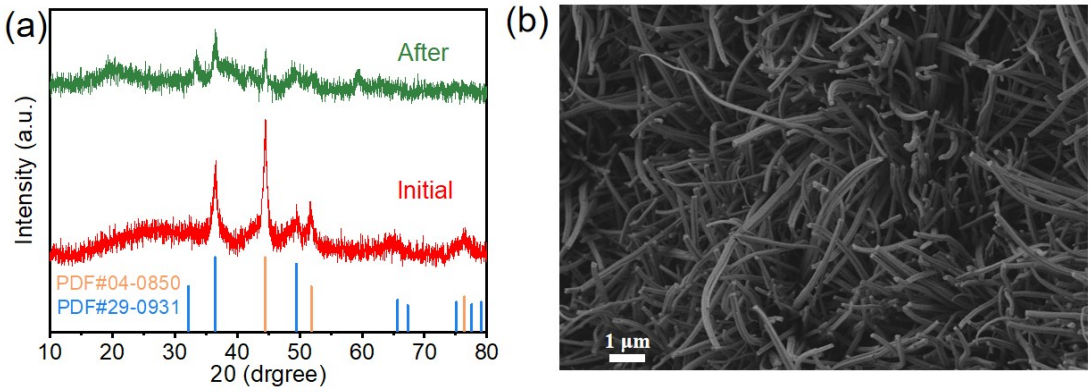

Fig. S8. (a) XRD spectra of the Fe-NiMoN catalyst and (b) SEM image for Fe-NiMoN after HER stability.

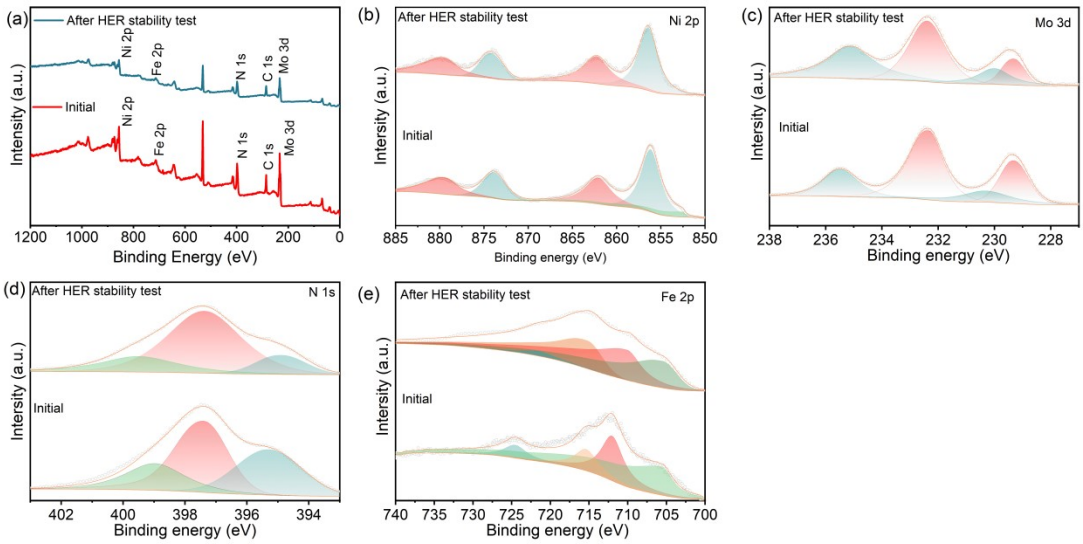

Fig. S9. XPS spectrum analysis. (a) XPS survey spectra of Fe-NiMoN before and after HER stability test. (b)、(c)、(d) and (e) are the high-resolution Ni 2p, Mo 3d and N 1s XPS spectra of Fe-NiMoN before and after HER stability test.

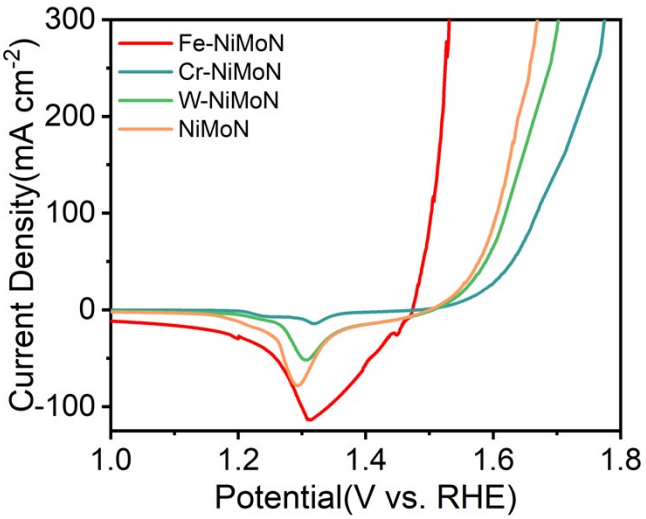

Fig. S10. Polarization OER curves of Fe-NiMoN, Cr-NiMoN, W-NiMoN and NiMoN.

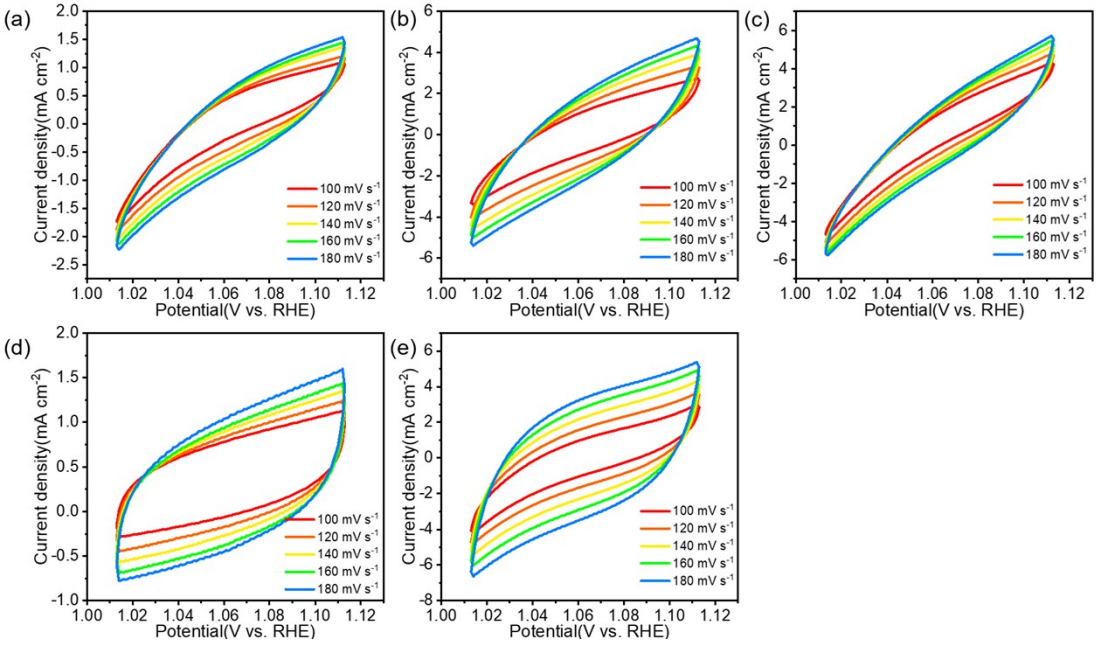

Fig. S11. CV curves of the catalysts recorded in the region of 1.013-1.113 V vs. RHE at different scan rates. (a) NF, (b) RuO_2, (c)NiMoN , (d) $NiMoO_4$, (e) Fe-NiMoN

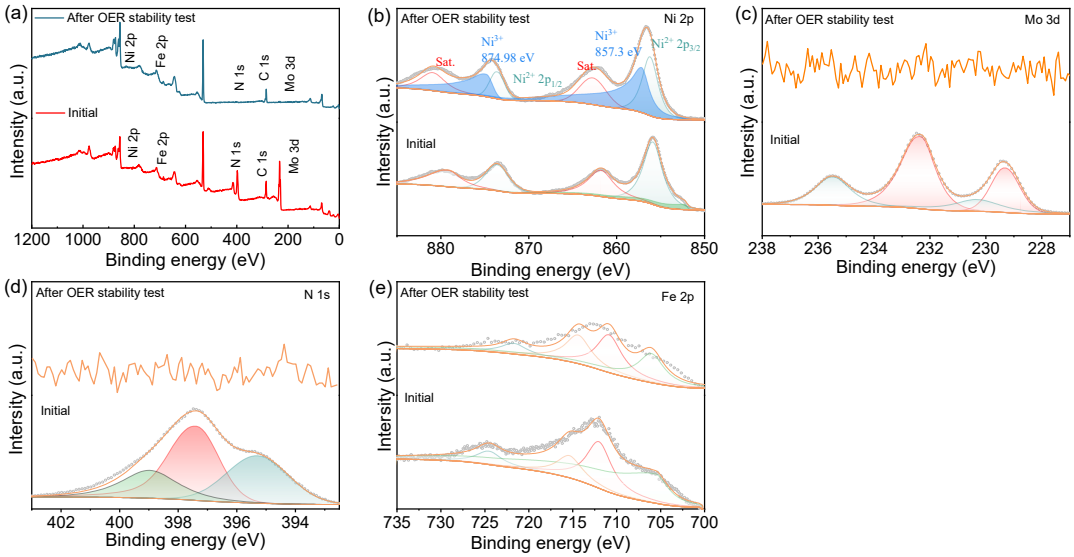

Fig. S12. XPS spectrum analysis. (a) XPS survey spectra of Fe-NiMoN before and after OER stability test. (b), (c) and (d) are the high-resolution Ni 2p, Mo 3d ,N 1s and Fe 2p XPS spectra of Fe-NiMoN before and after OER stability test.

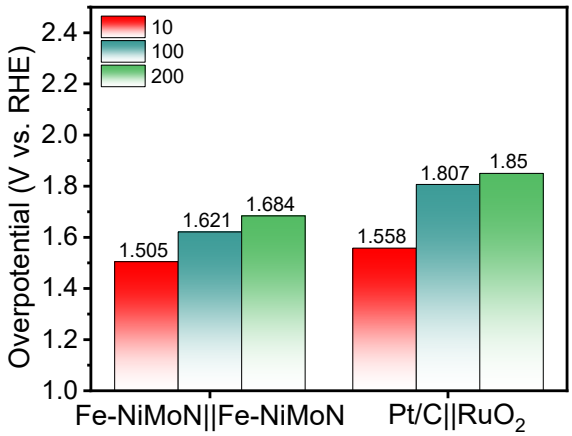

Fig. S13. Comparison of overpotential of as-prepared catalysts at different current densities (η =10, 100, 200 mA cm^{-2}).

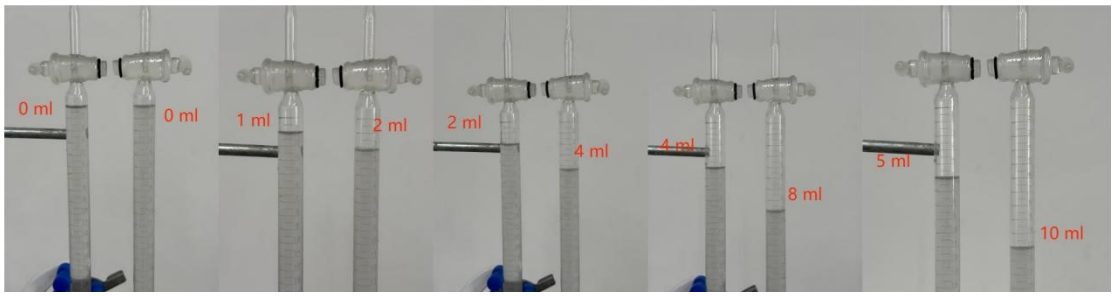

Fig. S14. Overall water splitting was performed in an improved Hoffman water electrolyzer; Corresponding levels of O_2 (left) and H_2 (right) gases generated at different times of 0 s (a), 1800 s (b), 3600 s (c), 7200 s (d), 9000 s (e) for Fe-NiMoN.

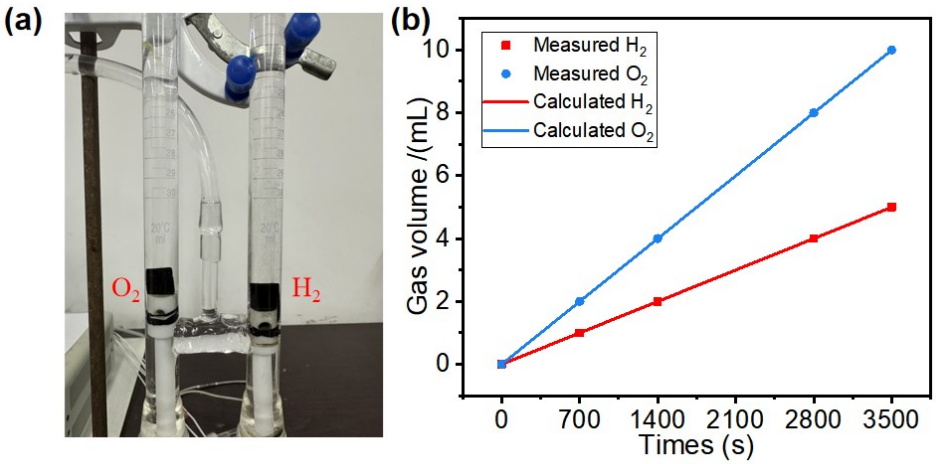

Fig. S15. (a) Pictures of the device for collecting O_2 and H_2, (b) Experimental and theoretical volumes of the generated O_2 and H_2 by the Fe-NiMoN.

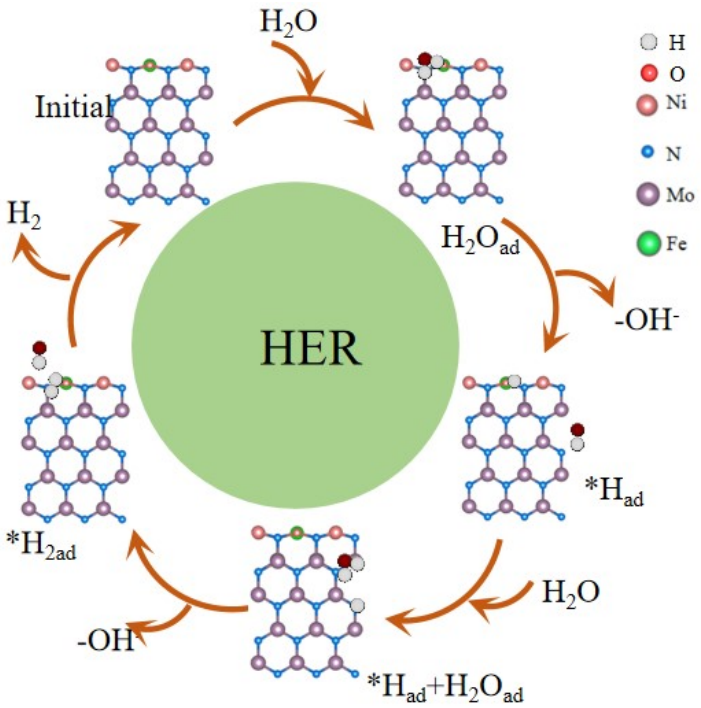

Fig. S16. The mechanism cycle diagram of HER on Fe-NiMoN in the alkaline media.

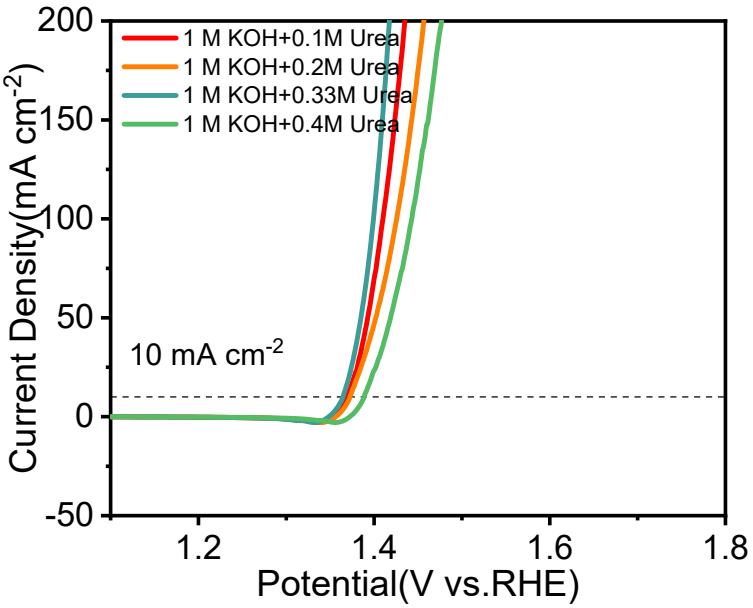

Fig. S17. The UOR performance of Fe-NiMoN in 1 M KOH with different Urea concentrations.

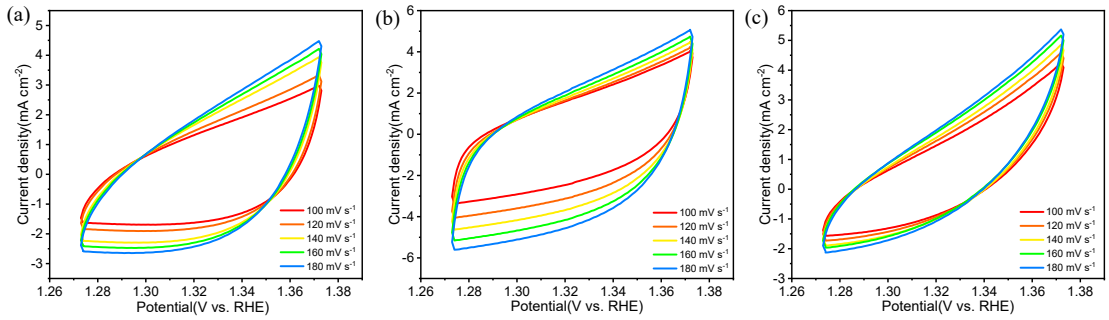

Fig. S18. CV curves of the catalysts recorded in the region of 1.273-1.373 V vs. RHE at different scan rates. (a) Fe-NiMoN, (b) NiMoN, (c) $NiMoO_4$.

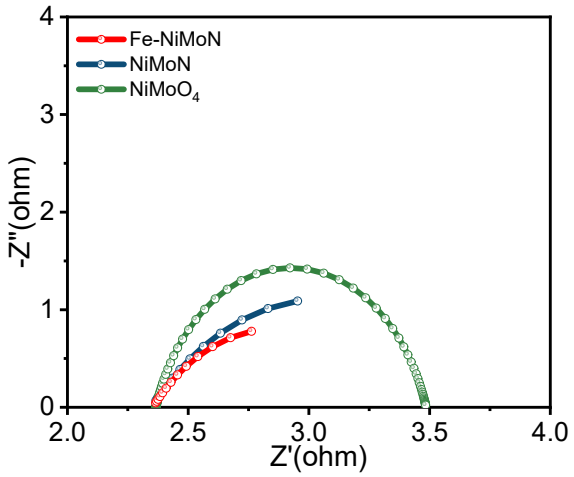

Fig. S19. Nyquist plots of the as prepared Fe-NiMoN, NiMoN, $NiMoO_4$ catalysts in 1 M KOH containing 0.33 M urea.

Table S1. Comparison of the performance for Fe-NiMoN with the recently reported HER electrocatalysts in 1 M KOH solution.

Catalysts	Cell voltage (V) at J=10 mA cm^{-2}	Mass loading (mg/cm^{-2})	References
Fe-NiMoN	**17**	**34**	**This work**
NiMoNx	78	36	Angew. Chem. Int. Ed. 2012, 51, 6131.
Mo_5N_6	94	66	ACS Nano. 2018, 12, 12761.
NiMoOx/NiMoS	38	38	Nat Commun. 2020, 11, 5462.
MoS_2/MoP nanorods	92	59.8	Small. 2020, 16, 2002482
P-MoP/Mo_2N	89	78	Angew. Chem. Int. Ed. 2021,60,6673-6681
Ni_2P/MoO_2/NF	34	46	Appl. Catal. B-Environ. 2020, 118803
Mo-NiPx/NiSy	85	73	Adv. Funct. Mater. 2021, 31, 2101532
Ni/NiMoN-30	48	75	Electrochimica Acta. 2022, 403, 139702
NiS_2/MoS_2 HNW	204	65	ACS Catal. 2017, 7, 6179-6187

Table S2. Comparison of the reported Transition-metal oxides-based or Transition-metal chalcogenides-based OER catalysts at a current density of 10 mA cm^{-2} in 1 M KOH.

Catalysts	Overpotential	References
Fe-NiMoN	**238**	**This work**
Ni_3FeN	270	*ACS Nano* 2018, 12, 245-253.
$Fe_{0.09}Co_{0.13}$-$NiSe_2$	290	*Mol. Catal*., 2022, 530, 112640.
Ru-Co3O4/CoP/TM	293	*Adv. Funct. Mater.* 2019, 29, 1807031.
NiFeCo-LDH	249	*Small* 2020, 16, 2002426.
$(Ni,Fe)S_2$@MoS_2/NF	270	*Appl. Catal. B* 2019,247, 107.
Ni_3S_2-NiOx/NF	241	*J. Colloid Interface Sci., 2022, 622, 728-737.*
NiFexSn@NiFe	260	*Adv. Sci.* 2020, 7, 1903777.
NiFe LDH	260	*Adv. Mater.* 2019, 31, 1903909.

Table S3. ICP-OES analysis of Ni, Mo and Fe elements content in electrolyte for Fe-NiMoN catalyst after OER stability testing.

Samples	Elemental content in electrolyte (μg/L)		
	Ni	Mo	Fe
Fe-NiMoN	6.3	262	12.4

Table S4. Comparison of the performance for Fe-NiMoN with the recently reported OER catalysts in 1 M KOH solution with 0.33 M urea.

Catalysts	Potential (V) at J=10 mA cm^{-2}	References
Fe-NiMoN	**1.369**	**This work**
NiFeMo	1.38	Appl. Surf. Sci. 552 (2021) 149514
Fe-Ni_3S_2@$FeNi_3$-8	1.4	Chem. Eng. J. 396 (2020) 125315
NiMoSe/NF	1.39	Int. J. Hydrogen Energy., 46 (2021) 37792-37801
$(Ni_{0.25}Fe_{0.75})_3S_2$/NF	1.38	ACS Appl. Energy Mater. 5 (2022) 1183-1192
Ce-Ni_2P	1.406	J. Alloys Compd. 912 (2022) 165234
Ni/MoC/Ti3C2Tx@C	1.56	ACS Appl. Energy Mater.6 (2023)1404–1412

Table S5. Comparison of different catalysts for overall water electrolysis and urea electrolysis.

Catalysts	Potential (V) at J=10 mA cm^{-2}	References
Fe-NiMoN	**1.467**	**This work**
Fe-Ni_3S_2@$FeNi_3$-8	1.5	Chem. Eng. J. 396 (2020) 125315
NiFeSbP/GB	1.54	ACS Appl. Energy Mater. 5 (2022) 15689-15700
Ni_2P/Ni	1.47	Nano Research 14 (2020) 1405-1412
CoS_2 NA/Ti	1.59	Electrochim. Acta 246 (2017) 776-782
S-NiMo/NF	1.574	Appl. Surf. Sci. 600 (2022) 154116
Fe-doped NiS – NiS_2	1.55	Small 18 (2022) 2106841